Optical Society of America. Ming Han and Anbo Wang, "Exact Analysis of Low-Finesse Multimode Fiber Extrinsic Fabry-Perot Interferometers," Appl. Opt. 43, 4659-4666 (2004). doi: 10.1364/ao.43.004659

Exact analysis of low-finesse multimode fiber extrinsic Fabry–Perot interferometers

Ming Han and Anbo Wang

A straightforward theory is presented to accurately model the light inferences in a low-finesse multimode fiber extrinsic Fabry–Perot (FP) interferometer. The effect on the fringe visibility of the gap length, sensor structure imperfections, and modal power distributions is explored. The analysis is particularly useful in the design and optimization of sensors that use an extrinsic FP cavity as the sensing element.

OCIS codes: 060.2370, 120.2230, 120.3180, 060.2310, 030.4070.

1. Introduction

Fiber-optic sensors have found numerous industrial and military applications in the past three decades. These sensors possess small size and high sensitivity, are immune to electromagnetic interference, and can be modified for distributed or multiparameter measurement. Among them, extrinsic Fabry–Perot (FP) interferometric (EFPI) fiber-optic sensors have attracted a great deal of attention because of their simple sensor structure and capability to measure various parameters such as strain,[1] temperature,[2] pressure,[3,4] and acoustic waves.[5] However, the generally relatively higher cost of fiber-optic sensors compared with their electronic counterparts has limited the widespread use of these sensors. One of the limiting factors is use of high-power broadband light sources for white-light interferometry that permits accurate and absolute measurement. Multimode fiber (MMF) EFPI sensors would significantly lower the cost of the sensor systems because MMFs impose less-stringent constraints on the light source. Furthermore, for extreme harsh environments with temperatures above 1000 °C, sapphire fiber EFPI sensors[6] are considered; these sapphire fibers are highly multimode because they are not clad and have a core size that is usually more than tens of micrometers.

The authors are with the Center for Photonics Technology, Bradley Department of Electrical and Computer Engineering, Virginia Polytechnic Institute and State University, Blacksburg, Virginia 24061-0111. The e-mail address for M. Han is mhan@vt.edu.

Received 19 January 2004; revised manuscript received 24 May 2004; accepted 26 May 2004.

0003-6935/04/244659-08$15.00/0

The FP cavity in an EFPI sensor is usually formed between the endface of a lead-in fiber and a reflector placed at a distance (usually less than a few hundred micrometers) to the lead-in fiber endface. The reflections at the lead-in fiber endface and at the reflector are coupled back to the lead-in fiber and interfere to form certain interferometric fringe patterns. Changes in the FP cavity length, known as the gap length, cause the interferometric fringe variations. For an intensity-based low-finesse EFPI sensor, the sensitivity to a measurand-induced change in gap length is highly dependent on the visibility of the fringes. The fringe visibility in single-mode fiber (SMF) EFPI sensors has been extensively analyzed by the modeling of the output of the fiber as a point source[7] or, more accurately, as a Gaussian beam.[8] However, the research on MMF EFPI sensors has been limited. Pérennès *et al.*[9] have analyzed the MMF EFPI sensors based on geometrical-optics theory, in which the output of the propagation modes in a MMF is modeled as incoherent rays outputting the fiber endface with different angles. The geometrical-optics theory is an approximate method and is adequate only when the fiber characteristic dimension is much larger than the optical wavelength. This condition may not be satisfied for strongly guiding fibers, in which the refractive-index difference between the core and the cladding is large, such as a sapphire fiber; however, the electromagnetic theory that is based on Maxwell's equations can, in principle, be used in any situation and provides a complete treatment on mode mixing and inference. Nevertheless, to the best of our knowledge, no theoretical research on the exact analysis of MMF EFPI sensors based on electromagnetic wave propagation has been reported in detail so far.

This paper is constructed as follows. In Section 2 we present an exact analysis on the fringe visibility of MMF EFPI sensors based on the electromagnetic theory. Even though a weakly guiding fiber is used in our analysis, the method we present is applicable for fibers of any kind. Then the numerical results based on the theory are discussed in Section 3. First, the effect on fringe visibility of the sensor parameters including the fiber core size, numerical aperture (NA) of the fiber, the modal power distribution in the lead-in fiber, and the gap length of the FP cavity is studied. Next, the effect of one of the typical interferometer imperfections, in which the two reflection surfaces of the FP cavity are not perfectly parallel to each other, is studied both theoretically and experimentally and the results are compared to validate the theory. Finally, several conclusions are given in Section 4.

2. Theory

A schematic of a low-finesse MMF EFPI sensor is shown in Fig. 1. The FP cavity is formed by the endface R_1 of the lead-in MMF and another reflection surface R_2. For an ideal EFPI sensor, R_1 and R_2 are perfectly parallel to each other and are perpendicular to the fiber axis z. n_3 is the refractive index inside the FP cavity. For simplicity, it is assumed that the cavity is filled with air and thus $n_3 = 1$. Suppose the MMF has a core radius a and is step indexed with a refractive index n_1 in the core and n_2 in the cladding. The gap length d is defined as the distance between R_1 and R_2. The reflection coefficient r_1 of surface R_1 and reflection coefficient r_2 of surface R_2 are defined by the weak Fresnel reflection arising from the refractive-index mismatches at the two surfaces. In practice, the reflections at the interfaces are usually small. The light propagating along the lead-in MMF is partially reflected by R_1 and R_2, and the two reflections are coupled back into the lead-in MMF and interfere to form interferometric fringes.

We assume that the MMF supports N orthogonal guided eigenmodes with the normalized field profile of the kth modes ϕ_k ($k = 1, 2, \ldots, N$). The total field of the light propagating along the $+z$ direction can be expressed as a superposition of all the guided modes, which can be written as[10]

$$\mathbf{E}_{\text{total}} = \sum_{k=1}^{N} p_k \phi_k \exp(-j\beta_k z)\hat{\mathbf{e}}_k = \sum_{k=1}^{N} |p_k| \exp(j\varphi_{pk})\phi_k \exp(-j\beta_k z)\hat{\mathbf{e}}_k, \quad (1)$$

where $\hat{\mathbf{e}}_k$ is a unit vector representing the polarization of the mode and the coefficient p_k is the complex magnitude of the kth mode representing the modal distribution in the fiber. For example, if we assume all modes in the MMF are equally excited, then all modes will have the same intensity, so $|p_k| = p$ for $k = 1, 2, \ldots, N$, where p is a constant. The intensity of the reflected light can be expressed as the superposition of the intensities of all modes because they are orthogonal:

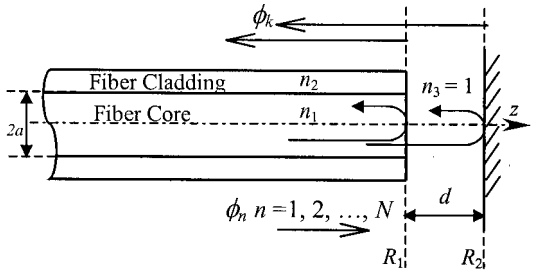

Fig. 1. Schematic of a low-finesse MMF EFPI sensor.

$$I = \langle \mathbf{E}_{\text{total}} \cdot \mathbf{E}_{\text{total}}^* \rangle = \sum_{k=1}^{N} (p_k\phi_k)(p_k\phi_k)^* \langle \hat{\mathbf{e}}_k \cdot \hat{\mathbf{e}}_k^* \rangle = \sum_{k=1}^{N} p_k p_k^* = \sum_{k=1}^{N} I_k. \quad (2)$$

Similarly, for the reflected light propagating along the $-z$ direction, the field can also be decomposed to a set of guided modes:

$$\mathbf{E} = \sum_{k=1}^{N} q_k \phi_k \exp(-j\beta_k z)\hat{\mathbf{e}}_k, \quad (3)$$

and the intensity of the reflected light is expressed as

$$I_R = \langle \mathbf{E} \cdot \mathbf{E}^* \rangle = \sum_{k=1}^{N} q_k q_k^* = \sum_{k=1}^{N} I_k. \quad (4)$$

Now we consider the field of a particular mode $q_k\phi_k$ of the reflected light. Because the Fresnel reflections at the reflection surfaces are low, the effect of the multiple reflections in the cavity is neglected. Thus the reflected light comes from the two reflections at surface R_1 and surface R_2. Because surface R_1 is perpendicular to the fiber axis, the kth mode propagating along the $+z$ direction will be coupled back to the kth mode propagating along the $-z$ direction at the reflection by surface R_1 and there is no coupling between modes with different mode numbers. However, because of the lateral displacement d (gap length) of surface R_2 to the fiber endface R_1, only part of the mode k propagating along the $+z$ direction that is reflected by surface R_2 can be coupled back to mode k. Furthermore, modes with mode numbers different from k that are reflected by surface R_2 can also be coupled into mode k. Thus the reflected field profile of mode k can be expressed as the summation of three terms:

$$q_k\phi_k = rp_k\phi_k + \eta_k rp_k\phi_k \exp(i\nabla\varphi_0) + c_k\phi_k \exp(i\nabla\varphi_{rk}). \quad (5)$$

Note that we have already assumed $r_1 = r_2 = r$ and neglected the light power loss due to the Fresnel reflection of surface R_1. In Eq. (5) the first term $rp_k\phi_k$ is the reflection at surface R_1; the second term $\eta_k rp_k\phi_k \exp(i\nabla\varphi_0)$ is the reflection at surface R_2 of the same mode k with a phase shift $\nabla\varphi_0 = 4\pi n_3 d/\lambda$ with respect to $\eta_k rp_k\phi_k$; η_k is the coupling coefficient be-

tween the mode k propagating along the $-z$ direction and the same mode propagating along the $+z$ direction but reflected back by surface R_2. The coupling occurs at the surface plane R_1. We assume $\eta_k = |\eta_k|\exp(i\varphi_k)$. The third term $c_k\phi_k \exp(i\nabla\varphi_{rk})$ is the reflection at surface R_2 of other modes with phase shift $\nabla\varphi_{rk}$, where c_k is an overall coupling coefficient and is a real number. Thus the reflected light intensity of mode k is expressed as

$$\begin{aligned} I_k &= q_k q_k^* \\ &= [rp_k + \eta_k rp_k \exp(i\nabla\varphi_0) + c_k \exp(i\nabla\varphi_{rk})] \\ &\quad \times [rp_k^* + \eta_k^* rp_k^* \exp(-i\nabla\varphi_0) \\ &\quad + c_k \exp(-i\nabla\varphi_{rk})] \\ &= r^2|p_k|^2 + r^2|\eta_k|^2|p_k|^2 + c_k^2 + 2r^2|\eta_k\|p_k|^2 \\ &\quad \times \cos(\nabla\varphi_0 + \varphi_k) \\ &\quad + 2r|p_k|c_k \cos(\nabla\varphi_{rk} - \varphi_{pk}) \\ &\quad + 2r|\eta_k\|p_k|c_k \cos(\nabla\varphi_0 + \varphi_k + \varphi_{pk} - \nabla\varphi_{rk}). \end{aligned} \tag{6}$$

Substituting Eq. (6) into Eq. (4) we obtain the total reflected light intensity I_R:

$$\begin{aligned} I_R &= \sum_{k=1}^{N} I_k \\ &= \sum_{k=1}^{N} [r^2|p_k|^2 + r^2|\eta_k|^2|p_k|^2 + c_k^2 \\ &\quad + 2r^2|\eta_k\|p_k|^2 \cos(\nabla\varphi_0 + \varphi_k) + 2r|p_k|c_k \\ &\quad \times \cos(\nabla\varphi_{rk} - \varphi_{pk}) + 2r|\eta_k\|p_k|c_k \\ &\quad \times \cos(\nabla\varphi_0 + \varphi_k + \varphi_{pk} - \nabla\varphi_{rk})]. \end{aligned} \tag{5}$$

Noting that all modes propagating along the MMF have a random initial phase relationship when they are excited by the light source and individual modes with different propagation constants experience a different phase shift during propagation along the fiber, it is reasonable to assume that $\nabla\varphi_{rk}$ is a random variable uniformly distributed in the phase range $[-\pi, \pi]$. Furthermore, we assume that the number of the modes excited in the fiber is sufficiently large so that the summation of the terms related to $\nabla\varphi_{rk}$ is averaged to zero in Eq. (7). This assumption is reasonable for a typical MMF that usually supports several hundred modes at wavelengths around 1550 nm. Thus Eq. (7) is simplified to be of the form

$$I_R = r^2 \sum_{k=1}^{N} |p_k|^2[1 + |\eta_k|^2 + c_k^2 + 2|\eta_k|\cos(\nabla\varphi_0 + \varphi_k)]. \tag{8}$$

Equation (8) is a function of the phase shift $\nabla\varphi_0$, and it describes the fringe visibility of the reflected light in the fiber. To find the maximum $I_{\max}$ and the minimum $I_{\min}$, the values of $\nabla\varphi_0$ where $I_{\max}$ and $I_{\min}$ occur are found when we solve

$$\partial I_R/\partial\nabla\varphi_0 = 0. \tag{9}$$

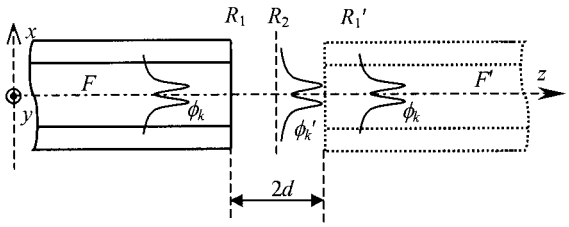

Fig. 2. Schematic of the calculation of η_{R_2} and η_k. Fiber F' is the mirror image of the lead-in fiber F with respect to the reflection surface plane R_2.

The solutions of Eq. (9) are given by

$$\nabla\varphi_{01} = -\tan^{-1}\left(\sum_{k=1}^{N} |p_k|^2|\eta_k|\sin\varphi_k \Big/ \sum_{k=1}^{N} |\eta_k|\cos\varphi_k\right), \tag{10}$$

$$\nabla\varphi_{02} = \pi - \tan^{-1}\left(\sum_{k=1}^{N} |p_k|^2|\eta_k|\sin\varphi_k \Big/ \sum_{k=1}^{N} |\eta_k|\cos\varphi_k\right), \tag{11}$$

one of which corresponds to $I_{\max}$ and the other to $I_{\min}$. Substituting Eqs. (10) and (11) into Eq. (8), we obtain $I_{\max}$ and $I_{\min}$:

$$\begin{aligned} I_{\max} &= r^2 \sum_{k=1}^{N} |p_k|^2[1 + |\eta_k|^2 + c_k^2 + 2|\eta_k\| \\ &\quad \times \cos(\nabla\varphi_{01} + \varphi_k)|], \end{aligned} \tag{12}$$

$$\begin{aligned} I_{\min} &= r^2 \sum_{k=1}^{N} |p_k|^2[1 + |\eta_k|^2 + c_k^2 - 2|\eta_k\| \\ &\quad \times \cos(\nabla\varphi_{01} + \varphi_k)|]. \end{aligned} \tag{13}$$

Thus the fringe visibility defined by $V_b = (I_{\max} - I_{\min})/(I_{\max} + I_{\min})$ is simply expressed as

$$V_b = \frac{2\sum_{k=1}^{N} |p_k|^2|\eta_k\|\cos(\nabla\varphi_{01} + \varphi_k)|}{\sum_{k=1}^{N} |p_k|^2 + \sum_{k=1}^{N} |p_k|^2(|\eta_k|^2 + c_k^2)}. \tag{14}$$

For simplicity, the input power of the lead-in fiber is normalized to be unity, namely,

$$I = \sum_{k=1}^{N} |p_k|^2 = 1. \tag{15}$$

Thus Eq. (14) is further simplified to be of the form

$$V_b = 2\sum_{k=1}^{N} |p_k|^2|\eta_k\|\cos(\nabla\varphi_{01} + \varphi_k)|/(1 + \eta_{R_2}), \tag{16}$$

where

$$\eta_{R_2} = \sum_{k=1}^{N} |p_k|^2(|\eta_k|^2 + c_k^2). \tag{17}$$

η_{R_2} is actually the light power coupling coefficient between the fiber F and its mirror image F' with respect to surface plane R_2, as shown in Fig. 2. For two step-index (SI) MMFs that have a longitudinal

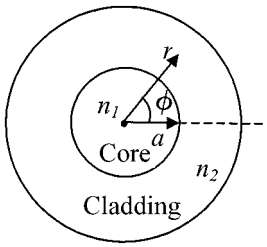

Fig. 3. Diagram of a cross section of the fiber geometry considered here.

offset $2d$, the light power coupling has been shown to be[11]

$$\eta_{R_2} = a^2/(a + 2d \tan \theta_c)^2, \tag{18}$$

where $\theta_c = \sin^{-1}[(n_1^2 - n_2^2)^{1/2}/n_1]$ is the critical acceptance angle of the fiber.

Now we consider the calculation of the mode coupling coefficient η_k. Assuming that ϕ_k' is the eigenmode ϕ_k of fiber F, transmitted a distance of $2l$ to plane R_1', the coupling coefficient is obtained when we perform the overlap integral of ϕ_k and ϕ_k' over the surface R_1', which leads to[9]

$$\eta_k = \iint_{R_1'} \phi_k' \phi_k^* \mathrm{d}x\mathrm{d}y. \tag{19}$$

The field distribution of ϕ_k' is given by the formula[12]

$$\phi_k'(x, y) = \mathbf{F}_{xy}^{-1}\{\mathbf{F}_{xy}[\phi_k(x, y)]H(k_x, k_y; z)|_{z=2d}\}, \tag{20}$$

where $\mathbf{F}_{xy}$ and $\mathbf{F}_{xy}^{-1}$ denote the two-dimensional spatial Fourier transform and its inverse Fourier transform with transform variables k_x and k_y known as spatial frequencies. $H(k_x, k_y; z)$ is called the spatial transfer function of propagation of light through a distance z in free space and is defined by[12]

$$H(k_x, k_y; z) = \exp\{-jk_0 z[1 - (k_x^2 + k_y^2)/k_0^2]^{1/2}\}. \tag{21}$$

The calculation of fringe visibility by Eq. (16) is general and applies to any MMF, provided that a sufficient number of modes is excited in the fiber. However, to keep the analysis as clear as possible and focused on the modes' interactions rather than calculations of the modes themselves, we assume here a weakly guided SI fiber, the structure of which is shown in Fig. 3. Because Δ is small, where $\Delta = (n_1 - n_2)/n_1$ is the normalized core–cladding index difference of the fiber, the linearly polarized mode approximation should be sufficient to describe the modes guided by the fiber.[13] With these assumptions, the characteristic equation in the fiber that we solve to obtain the effective index n_{eff} of all possible modes with azimuthal number l is given by[13]

$$J_l(u)/[uJ_{l-1}(u)] + K_l(w)/[wK_{l-1}(w)] = 0, \tag{22}$$

where J is a Bessel function of the first kind, K is a modified Bessel function of the second kind, u and w are defined by $u = (2\pi a/\lambda)(n_1^2 - n_{\mathrm{eff}}^2)^{1/2}$ and $w = (2\pi a/\lambda)(n_{\mathrm{eff}}^2 - n_2^2)^{1/2}$ at wavelength λ, and the rest of the parameters are defined in Fig. 3. Once Eq. (22) is solved, the field profile of an eigenmode in the fiber is readily obtained in terms of radial and azimuthal components[13]:

$$\phi_k = \begin{cases} A[J_l(ur/a)/J_l(u)]\sin(l\varphi + \varphi_0), & r < a \\ A[K_l(ur/a)/K_l(u)]\sin(l\varphi + \varphi_0), & r > a \end{cases}. \tag{23}$$

The number of guided modes that a fiber can support is determined by the normalized frequency V of the fiber, which is defined by $V = (2\pi a/\lambda)(n_1^2 - n_2^2)^{1/2}$. Provided that $l > 0$, the maximum value of l can be found when we solve the inequities

$$\begin{cases} J_{l-1}(V) < 0 \\ J_l(V) \geq 0 \end{cases}. \tag{24}$$

So far we have elaborated the calculations of the mode profiles ϕ_k; thus the mode coupling coefficient η_k can be obtained by a combination of Eqs. (20) and (19). From Eq. (16), modal distribution parameters $|p_k|^2$ are needed before the fringe visibilities can be calculated. A uniformly modal power distribution is assumed in many reports.[9,10] However, if we assume that the mode coupling through the propagation along the MMF is negligible, which may be a reasonable assumption for a fiber length no longer than several hundred meters,[14] $|p_k|^2$ can be calculated by the initial conditions and is given by

$$|p_k|^2 = B\left|\iint_{R_i} \phi_s \phi_k^* \mathrm{d}x\mathrm{d}y\right|^2, \tag{25}$$

where ϕ_s is the field profile transmitted to the MMF input plane R_i of the light from the source that excites the MMF, and B is a normalization coefficient determined by Eq. (15). In our simulation, in addition to the assumption of uniform modal power distribution, we also study the case in which the MMF is illuminated by a SMF output, thus the light power of the MMF has a heavier distribution on the lower-order modes.

3. Results

In this section the effect on the fringe visibility of the gap length of a sensor is first studied in Subsection 3.A. Then the effect of a typical imperfection in a MMF EFPI sensor, namely, the wedge of the sensor head, is studied theoretically in Subsection 3.B and experimentally in Subsection 3.C. In the analysis, the light wavelength is set to $\lambda = 1.55$ μm. Three different types of weakly guided SI MMF are chosen as the lead-in fiber in the MMF EFPI sensor, the parameters of which are shown in Table 1. Fiber 1 has a much larger core diameter ($2a$) than fiber 2; however, their core and cladding refractive indices n_1 and n_2 are chosen to support the same total linearly polarized mode number N in both fibers. Fiber 3 is

Table 1. Fiber Parameters Used in the Simulation

Parameter	Fiber 1	Fiber 2	Fiber 3
$2a$ (μm)	100	50	50
n_1	1.448	1.448	1.448
n_2	1.440	1.416	1.440
NA	0.15	0.30	0.15
V number	30.80	30.68	15.40
N	127	127	33

chosen to have the same core diameter as fiber 2 and the same n_1 and n_2 as fiber 1. Thus fiber 3 has the same NA as fiber 1, but a smaller V number and supports less modes than fibers 1 and 2.

A. Gap Length

Here we assume an ideal MMF EFPI sensor, with reflection surfaces R_1 and R_2 perfectly parallel to each other and both perpendicular to the fiber axis z. First we consider the case in which all the propagation modes in the MMFs are equally excited, which leads to $|p_k|^2 = 1/N$ according to Eq. (15). The fringe visibility as a function of the gap length for fibers 1, 2, and 3 is shown in Fig. 4. The fringe visibility of all three fibers starts from the same maximum (100%) at $d = 0$ and decreases as the gap length increases, with sidelobes appearing at the tail of the curves. However, the visibility of fiber 2, which has a larger NA than fibers 1 and 3, drops much more quickly down to the first minimum as the air gap increases to 16 μm. The visibility of fibers 1 and 3, which have the same NA, drops to its first minimum almost at the same gap length. This is in agreement with the conclusion obtained by the geometrical-optics theory[9] that the gap length $d_{\min}$, where minimum fringe visibility occurs, is determined by the NA of the fiber; a smaller NA leads to a larger $d_{\min}$.

Next the effect on the fringe visibility of the mode field distribution is considered. Instead of a uniform modal power distribution, we consider the case in which the MMF is illuminated by a SMF output, as shown in Fig. 5. In our simulation, the SMF has a core refractive index of 1.445, a cladding refractive index of 1.440, and a core diameter of 9 μm. There is only one mode, ϕ_0, propagating along the SMF, and the calculated mode field diameter is 10.04 μm. From Eq. (25), only those modes with the same azimuthal number as ϕ_0 can be excited in the MMF. Thus only a portion of guided modes are excited. The mode power coefficient of each mode, $|p_k|^2$, is given by Eq. (25), and the calculated fringe visibility as a function of gap length is shown in Fig. 6.

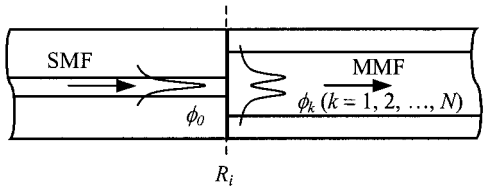

Fig. 5. Schematic of a MMF illuminated by a SMF output.

A comparison of Figs. 6 and 5 shows that, for a given gap length, the MMF EFPI sensor excited by a SMF has a larger fringe visibility compared with a uniform mode excitation. For example, fiber 2 illuminated by a SMF still has a fringe visibility of 71.8% at the gap length of 16 μm, whereas it would drop to only 6.0% if all modes were uniformly excited. Also note that the fringe visibility of fiber 1 drops slower than that of fiber 3 in Fig. 6, whereas they have almost the same response to the gap length when all modes are uniformly excited. This indicates that a reduction in mode numbers is more efficient for larger core fibers to increase the fringe visibility.

B. Wedges

In practice, the two reflection surfaces in a MMF EFPI sensor are usually not perfectly parallel to each other because of the limited fabrication accuracy. The cavity geometry therefore becomes that of a wedge, introducing variations in the cavity thickness of the interferometer. The effect on fringe visibility of the wedge is studied in this subsection. Here we

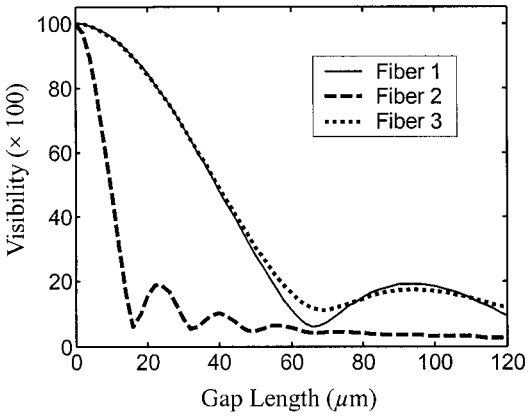

Fig. 4. Fringe visibility versus gap length for fibers 1, 2, and 3. All modes in the MMFs are equally excited.

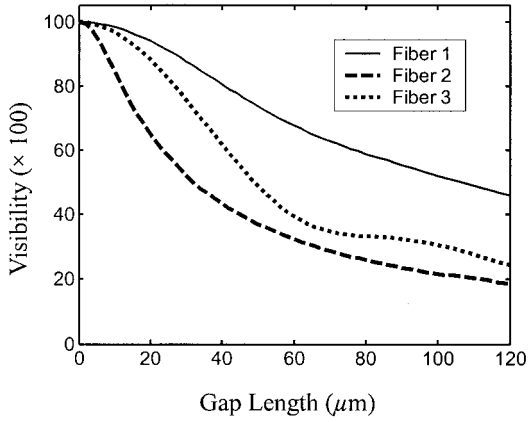

Fig. 6. Fringe visibility versus gap length for fibers 1, 2, and 3. The MMF are illuminated by a SMF output.

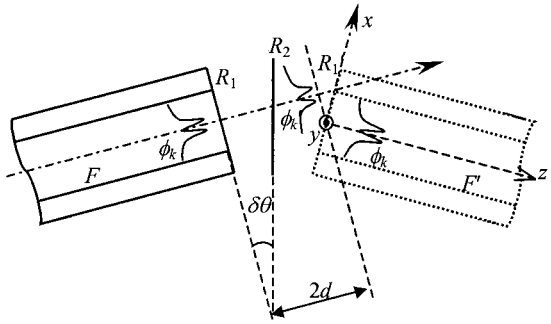

Fig. 7. Illustration of a MMF EFPI sensor with a wedge between the two reflection surfaces R_1 and R_2. Fiber F' is the mirror image of fiber F with respect to surface plane R_2.

assume that reflection surface plane R_1 is still perpendicular to the fiber axis z whereas reflection surface R_2 is tilted from its original position, forming a wedge angle of $\delta\theta$ with respect to R_1, as shown in Fig. 7. The effect of the angular and lateral misalignment between the lead-in fiber F and its mirror image fiber F' caused by a wedge must be considered when we use Eq. (19) to calculate the mode coupling coefficient η_k. The effect of the wedge is to produce a linear phase change across the beam[15] and a spatial displacement between mode ϕ_k' and ϕ_k at the coupling plane R_1'. For mode ϕ_k' that is misaligned by a wedge angle $\delta\theta$, the field can be described by

$$\phi_{k,\delta\theta}'(x, y) = \phi_k'(x - 2d \tan\theta, y) \times \exp[jk_0 x \tan(2\delta\theta)]. \quad (26)$$

Thus mode coupling coefficient η_k is obtained when Eq. (26) is substituted into Eq. (19).

Again we assume that all the modes are equally excited in the fiber. The fringe visibility of fiber 1 as a function of the wedge angle is plotted in Fig. 8 at different gap lengths d = 20, 30, and 40 μm. The fringe visibility curve decreases as the wedge angle is increased and it also shows sidelobe structures at the tail of the curve. It is also shown that, even with

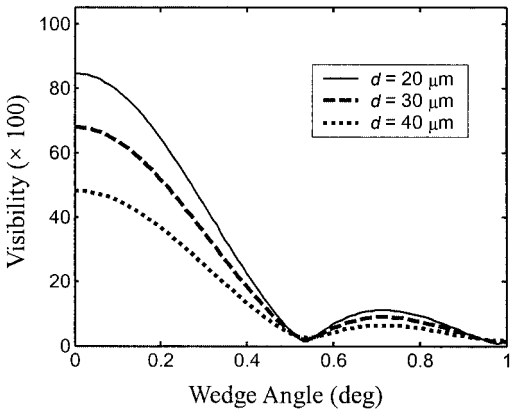

Fig. 8. Fringe visibility versus wedge angle for fiber 1 at a gap length d = 20, 30, and 40 μm. All modes in the MMFs are equally excited.

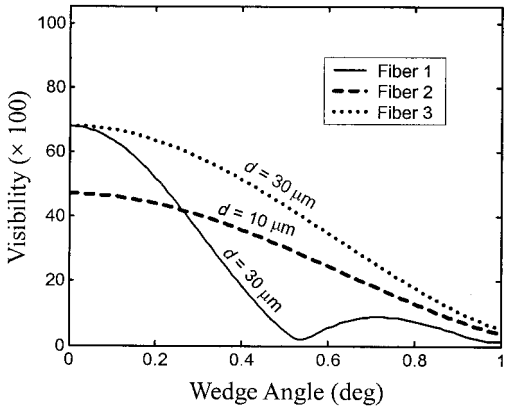

Fig. 9. Fringe visibility versus wedge angle for fibers 1, 2, and 3. All modes in the MMFs are equally excited.

different starting visibilities, the three curves corresponding to various gap lengths drop to the first minimum, which is around 4%, at the same wedge angle of 0.54°. Thus the effect on the fringe visibility of the wedge angle does not depend on the gap length. The fringe visibility for the three fibers at selected gap lengths is plotted in Fig. 9. The gap length used for fibers 1 and 3 are 30 μm, whereas a 10-μm gap length is used for fiber 2 to clearly show the trend of fringe visibility changes. Apparently the fringe visibility curve of fiber 1 drops more quickly than fibers 2 and 3, whereas the fringe visibility of fibers 2 and 3 shows a similar response to the wedge angles. Thus it is concluded that the sensitivity of fringe visibility to wedge angle depends on the fiber core diameter. A MMF EFPI sensor with bigger core diameter fibers is more vulnerable to imperfections on the parallelism of the two reflection surfaces of the cavity.

Now we consider the case in which the MMF is illuminated by a SMF output, as discussed in Subsection 3.A. The SMF parameters are all the same as those in Subsection 3.A. The results for fibers 1, 2, and 3 are shown in Fig. 10 and compared with the result shown in Fig. 9. The comparison shows that the sensitivity of fringe visibility to the wedge angles

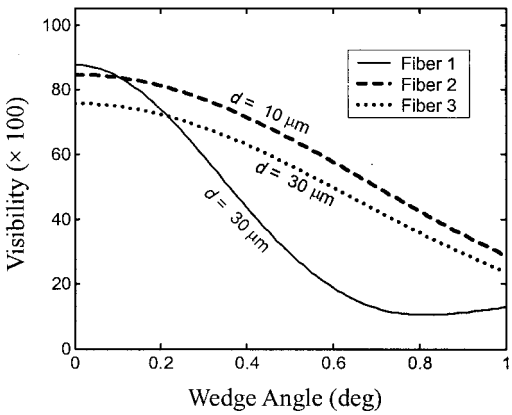

Fig. 10. Fringe visibility versus wedge angle for fibers 1, 2, and 3. The MMFs are illuminated by a SMF output.

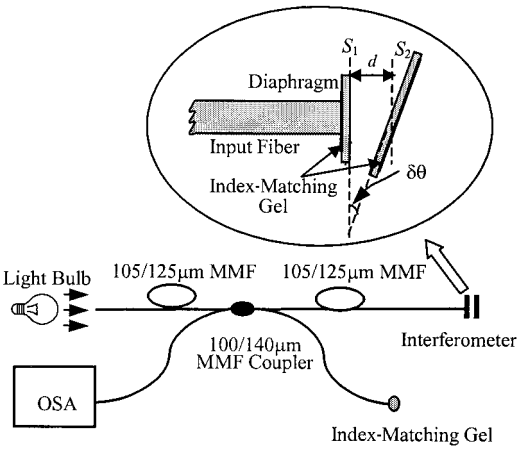

Fig. 11. Experimental setup to measure the fringe visibility as a function of wedge angle. OSA, optical spectrum analyzer.

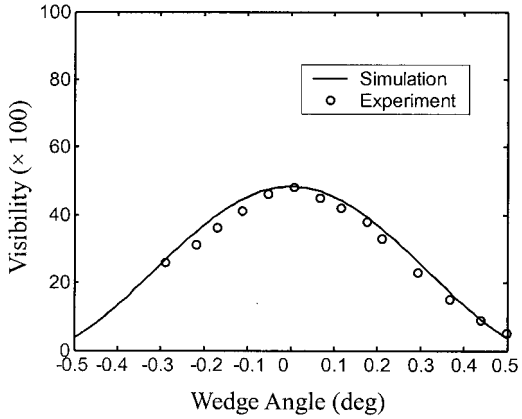

Fig. 12. Comparison between the theoreticals and the experimental results on the fringe visibility versus wedge angle.

is not significantly effected when the modes are reduced in number, even though fringe visibility is increased by SMF output excitation.

C. Experimental Verification

To validate the theory and the analysis, the fringe visibility as a function of the wedge angle was measured to compare with the theoretical results. The experimental setup is shown in Fig. 11. To maximally excite the modes of the MMF, the light from a fiber-optic light system (Model MKII, Nikon, Inc.) was directly coupled into 1-m-long SI MMF with a core diameter of 105 μm and a cladding diameter of 125 μm. The refractive indices of the core and cladding in the fiber are 1.448 and 1.440, respectively. A 3-dB SI MMF coupler was used to separate the input and output light from the EFPI instrument. The core and cladding diameters of the fiber used for the coupler were 100 and 140 μm, respectively. Another 1-m-long 105–125-μm SI MMF was used to transmit the input and output light to and from the interferometer. The detail of the interferometer is shown in the inset of Fig. 11. To ensure that the two reflection surfaces are flat, instead of using a cleaved fiber end as the reflection surface, we attached a 50-μm-thick fused-silica substrate to the fiber end. Thus the side S_1 of the substrate formed one reflection surface of the EFPI instrument. The other reflection surface was formed by the side S_2 of a 170-μm-thick fused-silica substrate, which is mounted onto a five-dimensional positioner to allow the adjustment of the wedge angle δθ. Index-matching gel was applied to the fiber end and to the sides of the diaphragms where reflections are undesirable. An optical spectrum analyzer (Model AQ-6315A, Ando Electric Co., Ltd.) was used to measure the interference fringes from the EPFI instrument and monitor the gap length d. In the experiment, the wedge angle was changed from $-0.3°$ to $+0.5°$, and the gap length was maintained at 40 μm during the measurement. The experimental data for the visibility as a function of the wedge angle are plotted and compared with the theoretical result in Fig. 12. The theory and the analysis were validated by the good agreement between the experimental and the theoretical results.

4. Conclusions

A straightforward theory has been presented that accurately models the light inference in a low-finesse MMF EFPI sensor. In the model, the electric field is described by a set of guided modes with a certain power distribution and random phase relationship. The light inference occurs only on the same mode, whereas different modes could mix when the reflected light is coupled back to the fiber. Theoretically, this model is general and is sufficient to describe EFPI instruments with fibers of any kind.

On the basis of this model, our analysis shows that the fringe visibility decreases as the gap length increases. The analysis also indicates that the fringe visibility of an EFPI instrument with a smaller NA fiber is less sensitive to the gap length of the EFPI instrument. The wedge angle effect on fringe visibility is studied and is found to depend on the fiber core size. Fringe visibility is more sensitive to the wedge angle for a larger core MMF EFPI sensor. For example, for the 100-μm core diameter fiber EFPI sensor with a gap length of 30 μm, a 0.58° wedge angle will drop the fringe visibility to 4% if the all modes are equally excited. This corresponds to a 1.88-μm variation of the cavity thickness over the overall fiber core cross section.

Our analysis also indicates that the effect of the modal power distribution in the lead-in fiber could be significant. For a given gap length, the fringe visibility can be increased by a reduction of the number of modes excited in the fiber. This could be of great importance for cases in which it is difficult to reduce the NA of the fiber, for example, when sapphire fiber, which is not clad, is used.

References

1. C. Belleville and G. Duplain, "White-light interferometric multimode fiber-optic strain sensor," Opt. Lett. **18,** 78–80 (1993).
2. C. E. Lee and H. F. Taylor, "Fiber-optic Fabry-Perot temper-

ature sensor using a low-coherence light source," J. Lightwave Technol. **9,** 129–134 (1991).
3. A. Wang, H. Xiao, J. Wang, Z. Wang, W. Zhao, and R. G. May, "Self-calibrated interferometric-intensity-based optical fiber sensors," J. Lightwave Technol. **19,** 1495–1501 (2001).
4. Y. Kim and D. P. Neikirk, "Micromachined Fabry-Perot cavity pressure transducer," IEEE Photon. Technol. Lett. **7,** 1471–1473 (1995).
5. N. Furstenau, M. Schmidt, H. Horack, W. Goetze, and W. Schmidt, "Extrinsic Fabry-Perot interferometer vibration and acoustic sensor systems for airport ground traffic monitoring," IEE Proc. Optoelectron. **144,** 134–144 (1997).
6. H. Xiao, J. Deng, G. Pickrell, R. G. May, and A. Wang, "Single-crystal sapphire fiber-based strain sensor for high-temperature applications," J. Lightwave Technol. **21,** 2276–2283 (2003).
7. A. K. Murphy, M. F. Gunter, A. M. Vengsarker, and R. O. Claus, "Quadrature phase-shifted, extrinsic Fabry-Perot optical fiber sensors," Opt. Lett. **16,** 273–275 (1991).
8. V. Arya, M. J. de Vries, K. A. Murphy, A. Wang, and R. O. Claus, "Exact analysis of the EFPI optical fiber sensor using Kirchhoff's diffraction formalism," Opt. Fiber Technol. **1,** 380–384 (1995).
9. F. Pérennès, P. C. Beard, and T. N. Mills, "Analysis of a low-finesse Fabry–Perot sensing interferometer illuminated by a multimode optical fiber," Appl. Opt. **38,** 7026–7034 (1999).
10. C. M. Miller, S. C. Mettler, and I. A. White, *Optical Fiber Splices and Connectors: Theory and Methods* (Marcel Dekker, New York, 1986).
11. G. Keiser, *Optical Fiber Communications* (McGraw-Hill, Boston, Mass., 2000).
12. T.-C. Poon and P. R. Banerjee, *Contemporary Optical Image Processing with MATLAB* (Elsevier Science, New York, 2001).
13. A. Safaaii-Jazi, "Optical waveguides," Lecture notes (Department of Electrical and Computer Engineering, Virginia Polytechnic Institute and State University, Blacksburg, Va., 2002).
14. J. N. Kutz, J. A. Cox, and D. Smith, "Mode mixing and power diffusion in multimode optical fibers," J. Lightwave Technol. **16,** 1195–1202 (1998).
15. D. T. Neilson, "Tolerance of optical interconnections to misalignment," Appl. Opt. **38,** 2282–2290 (1999).